Acta Biomaterialia 6 (2010) 331–343

Contents lists available at ScienceDirect

Acta Biomaterialia

journal homepage: www.elsevier.com/locate/actabiomat

Toucan and hornbill beaks: A comparative study

Yasuaki Seki, Sara G. Bodde, Marc A. Meyers *

Department of Mechanical and Aerospace Engineering, Materials Science and Engineering Program, University of California, San Diego, La Jolla, CA 92093-0411, USA

ARTICLE INFO

Article history:
Received 2 May 2009
Received in revised form 16 August 2009
Accepted 19 August 2009
Available online 21 August 2009

Keywords:
Toucan beak
Hornbill beak
Sandwich structure
Brazier moment

ABSTRACT

The structure and mechanical behavior of Toco Toucan (*Ramphastos toco*) and Wreathed Hornbill (*Rhyticeros undulatus*) beaks were compared. The beak of both species is a sandwich-structured composite, having an exterior, or rhamphotheca, consisting of multiple layers of keratin scales and a core composed of a fibrous network of bony closed-cell foam. The rhamphotheca is an arrangement of ~50 μm diameter, overlapping, keratin tiles. The hornbill rhamphotheca exhibits a surface morphology on the ridged casque that is distinguishable from that observed on the bill proper. Intermediate filaments in the keratin matrix were observed by transmission electron microscopy. The Young's modulus measurements of toucan rhamphotheca indicate isotropy in longitudinal and transverse directions, whereas those of hornbill rhamphotheca may suggest anisotropy. The compressive response of beak foam is governed by brittle crushing behavior. The crushing strength of hornbill foam is six times higher than that of toucan foam. Micro- and nanoindentation hardness values were measured for rhamphotheca and foam trabeculae of toucan and hornbill specimens. The sandwich design of beaks was analyzed using the Karam–Gibson and Dawson–Gibson models. The presence of a cellular core increases the bending resistance (Brazier moment) by a factor of 3–6 while decreasing the compressive strength by only 50%.

1. Introduction

The study of biological materials has received much attention in recent years [1–5]. Avian materials (feathers, bones, beaks, claws) are remarkable as structural biological materials because of their low weight, requisite for flight in most birds, balanced by structural support or robustness for survival and social activities. The toco toucan (*Ramphastos toco*) and the wreathed hornbill (*Rhyticeros undulatus*) possess distinctively long and thick beaks. The bill of toco toucan is one-third of the total length of the bird, and hornbill beak is a quarter of the total length. The toucan beak is light in weight, comprising one-thirtieth to one-fortieth of the total mass of the bird; the hornbill beak is one-thirtieth of the total mass.

The beaks of toucan and hornbill can be described as a sandwich-structured composite. The exterior shell, or rhamphotheca, is made of β-keratin tiles. The internal foam consists of a fibrous network of trabeculae. These two components are separated by the dermis. Seki et al. [6,7] demonstrated that the buckling resistance of the beak is enhanced by the internal cellular core due to the synergism between the two components. The hollow foam affords increased energy absorption capacity with its low-density structure. The beak and feeding ecology of the Wreathed Hornbill seem to be similar to those of the Toco Toucan – an example of convergent evolution. In this study, the previous investigations of toco toucan beak by Seki et al. [6,7] were extended to the mechanical properties and microstructure of wreathed hornbill beak to compare the structure and function of the bill of a New World species to that of an Old World species filling a similar ecological niche.

2. Experimental techniques

Both toco toucan and wreathed hornbill beaks were obtained after the natural death of the birds and stored in a desiccator at 50% relative humidity (RH) and 20 °C. The toucan beaks were acquired from a private aviculturist at the Emerald Forest Bird Gardens in Fallbrook, California; Wreathed Hornbill beaks were from the San Diego Wild Animal Park of the San Diego Zoo. Because of limited specimen availability, or in some cases limited information on the host, no attempt was made to correlate the results with gender or age of the bird. The apparent density of the beak was computed as the mass, measured by digital balance, divided by the volume, which was estimated by measuring the volume displacement upon submersion of the specimen in water, therefore including the volume of some of the voids in the structure. Sections of beak rhamphotheca and foam were excised using a jeweler's handsaw and knife. The samples were mounted in epoxy and glued on glass plates for nano- and microhardness testing. The procedure for indentation was the same as that described previously for hardness

* Corresponding author. Address: Department of Mechanical and Aerospace Engineering, Materials Science and Engineering Program, University of California, San Diego, 9500 Gilman Drive, La Jolla, CA 92093-0411, USA. Tel.: +1 858 534 4719; fax: +1 858 534 5698.
E-mail address: mameyers@ucsd.edu (M.A. Meyers).

1742-7061/$ - see front matter © 2009 Acta Materialia Inc. Published by Elsevier Ltd. All rights reserved.
doi:10.1016/j.actbio.2009.08.026

measurement by Seki et al. [6,7]. A LECO M-400-H1 hardness testing machine was used for microindentation, applying loads of 100 gf. The authors used the same procedure (based on that described by Hillerton et al. for chitinous insect cuticle [8]) that Bonser and Witter employed for measuring the microhardness of starling beak keratin [9], by which the indentation load was applied for 15 s and then retracted, and after a further 45 s the diagonals of the indentation were measured, in an attempt to minimize effects of viscoelastic creep during measurement [8,10]. The hardness measurements were conducted at ambient conditions (48% RH and 20 °C). Since nanoindentation is highly sensitive to the roughness of the sample, specimens were polished with 0.05 μm alumina powder. A Hysitron Triboindenter was used to measure nanohardness, from which the reduced Young's modulus and the hardness of beak keratin and trabeculae of the interior were determined. Loads of 0.5 and 1 mN (Berkovich-type indenter) were applied to samples during nanoindentation.

The sample preparation for tensile testing of rhamphotheca was the same as the procedure described by Seki et al. [6,7]. The dimensions of dogbone-shaped samples were 25.4 mm in length and 2.3 mm in width, with a gauge length of 6.35 mm. Universal tensile machines (United, with a 220 N load cell, and Instron model 3342, with a 500 N load cell) were used to measure the tensile response of the rhamphotheca. The tests were carried out at room temperature and 48% RH. The cross-head speed was 0.40 mm min^{-1}, constituting a strain rate of 1×10^{-3} s^{-1}.

For compression testing, foam sections were cut by handsaw, and the rhamphotheca was stripped. The height of the samples was 1.5 cm and the cross-head speed was 1.27 mm min^{-1}. The cross-sectional area of foam samples was ~4.5 cm^2.

The topography of the rhamphotheca and the geometry of the trabecular foam were studied by imaging techniques. We employed scanning electron microscopy (SEM) with energy dispersive X-ray (EDX) spectrometry (FEI Quanta 600 and Phillips XL30), for structural and elemental analysis, respectively. The working distance was 10–15 mm and the voltage setting of the scanning electron microscope was 10–20 kV. Samples were imaged uncoated in an environmental scanning electron microscope or coated with either gold–palladium or chromium alloy.

X-ray computed tomography was used to study and reproduce the foam structure, for the purpose of stability analysis. We also used microcomputed tomography (μ-CT), using a G.E. eXplore RS rodent CT scanner. The μ-CT scans were conducted using an unfiltered X-ray source at 80 kV and 450 μA with exposure times of 100 ms. The three-dimensional interior foam structure was visualized by VTK (Visualization Toolkit) software [11], and we implemented a ray casting algorithm for volumetric rendering. The DICOM images, captured by 93, 43 and 27 μm resolution μ-CT, were converted to TIFF format and rescaled using ImageJ. The model was created from the six sets of stitched images for the maxillary beak and the five sets of stitched images for the mandibular beak. A segment of toucan beak foam was scanned at a resolution of 27 μm; hornbill casque was scanned at a resolution of 45 μm.

The nanostructure of the rhamphotheca was imaged by transmission electron microscopy (TEM). Rhamphotheca specimens were transversely sectioned and soaked in water for 2 h. The samples were fixed in 2.5% glutaraldehyde in 0.2 M phosphate-buffered saline (PBS) overnight. After rinsing with PBS, the samples were post-fixed in osmium tetroxide for 5 h and washed with water. Before the dehydration process, the samples were soaked in uranyl acetate overnight. They were then dehydrated in ethanol and polymerized with resin. The polymerized samples were baked in an oven at 50 °C for 48 h. After baking, they were longitudinally and transversely sectioned by ultramicrotome (Reichert-Jung UltracutE) to samples with 80 nm in thickness. A transmission electron microscope (JEOL-1200 (120 kV)) at the National Center for Microscopy and Imaging Research (NCMIR) facility was used to image the keratin structure.

3. Results and discussion

3.1. Structure of the beak

Fig. 1(a) is a photograph of the toucan beak. The apparent density of the toucan beak is approximately 0.1–0.2 g cm^{-3}. The outer shell, or rhamphotheca, of the beak is composed of β-keratin and encases a bony, interior foam. The hard, thin exterior enveloping the thick, low-density interior comprises the sandwich-structured composite. Fig. 1(b) shows a photograph of the hornbill beak. The density of the beak of hornbill is approximately 0.3–0.4 g cm^{-3}. The ridged helmet-like feature at the base of the maxilla is called the casque. We observed a unique topography in microstructure, to be discussed below, at the proximal terminus of the maxillary rhamphotheca, or rhinotheca, corresponding to the onset of the casque.

3.1.1. Scanning electron microscopy

Fig. 2(a) shows a scanning electron micrograph of the lateral surface of the toucan rhamphotheca. The polygonal keratin tiles have a thickness of ~1 μm and a diameter of ~45 μm. The total thickness of the toucan rhamphotheca is approximately 0.5 mm. Fig. 3(a) is a scanning electron micrograph of the hornbill rhamphotheca. The geometry of the keratin tiles is irregular compared to those observed on the toucan rhamphotheca, having dimensions of about 20 × 50 μm. The total thickness of the hornbill shell varies from the proximal to the distal termini from 1 to 2 mm, the thickness increasing toward the distal end of beak, with the exception of the casque. In the microstructure of the casque ridges, as depicted in Fig. 3(d), tiles and tile boundaries are not visible as they are on the toucan rhamphotheca and surrounding the hornbill rhamphotheca. The casque surface microstructure is distinguishable by carbon-rich, undulating ridges, as is evident in Fig. 4(b). Less than 1% calcium was detectable by EDX on the general rhamphotheca keratin for both the toucan and the hornbill. In contrast, the keratin deposited on the ridges of the hornbill casque contains more than 1% of calcium, based on EDX analysis. Fig. 4(a) shows a scanning electron micrograph with X-ray dot mapping of calcium. The calcium is homogeneously distributed on the toucan rhamphotheca. Fig. 4(b) shows scanning electron micrographs with X-ray dot mapping on hornbill ridges. The substance observed on the casque's surface contains more carbon than the keratin tile surface, whereas there is no significant difference in distribution of calcium.

Figs. 2(a) and 3(b) depict the interior foam of the toucan and hornbill beaks, respectively. The foam exhibits a closed-cell structure, as cell edges are joined by thin membranes. The average edge connectivity, as defined by Gibson and Ashby [12], is the number of edges that meet a vertex. For both toucan and hornbill foam, the edge connectivity was found to be approximately 3, as counted using scanning electron micrographs. The rod-like trabeculae are circular or elliptical in cross-section. The typical cell diameter of toucan and hornbill foam is on the order of millimeters. In the case of the hornbill foam, the trabeculae are thicker compared to those features observed in toucan foam. As corroborated by micro-CT data (Table 1), particularly the trabecular separation (TbSp) parameter, the variability in the cell size of toucan foam is greater than that of hornbill foam. The trabeculae of the foam contain 15–33% calcium as detected by EDX.

3.1.2. Transmission electron microscopy

Figs. 5 and 6 show transmission electron micrographs of longitudinal and transverse sections of toucan and hornbill rhamphot-

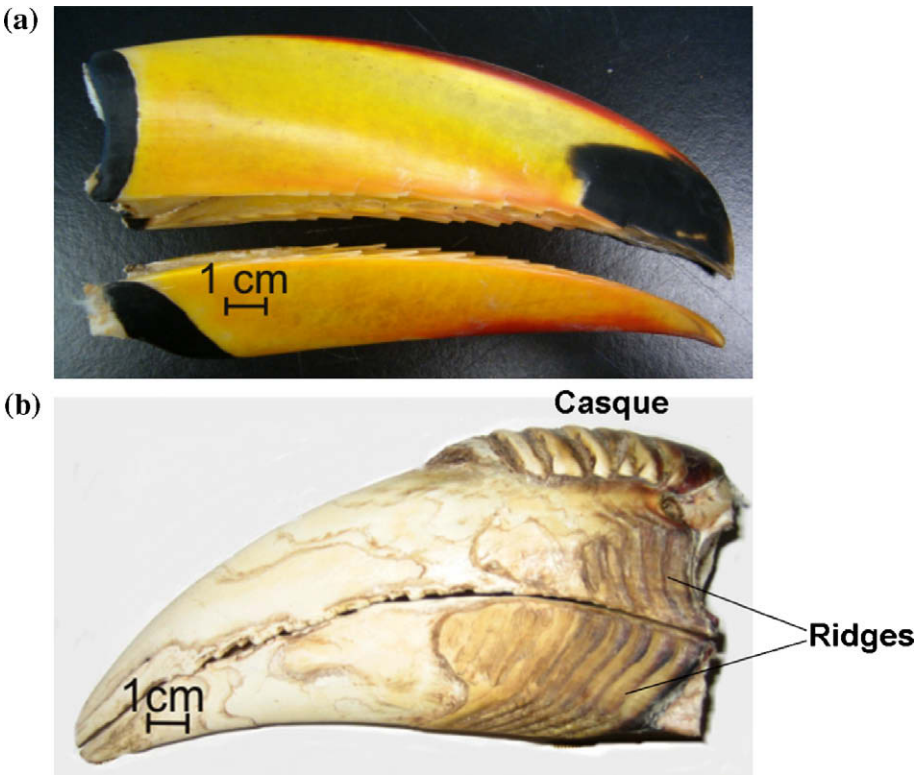

Fig. 1. Photographs of beak specimens used in this study: (a) maxillary (upper) and mandibular (lower) beak of toucan; (b) maxillary and mandibular beak of hornbill.

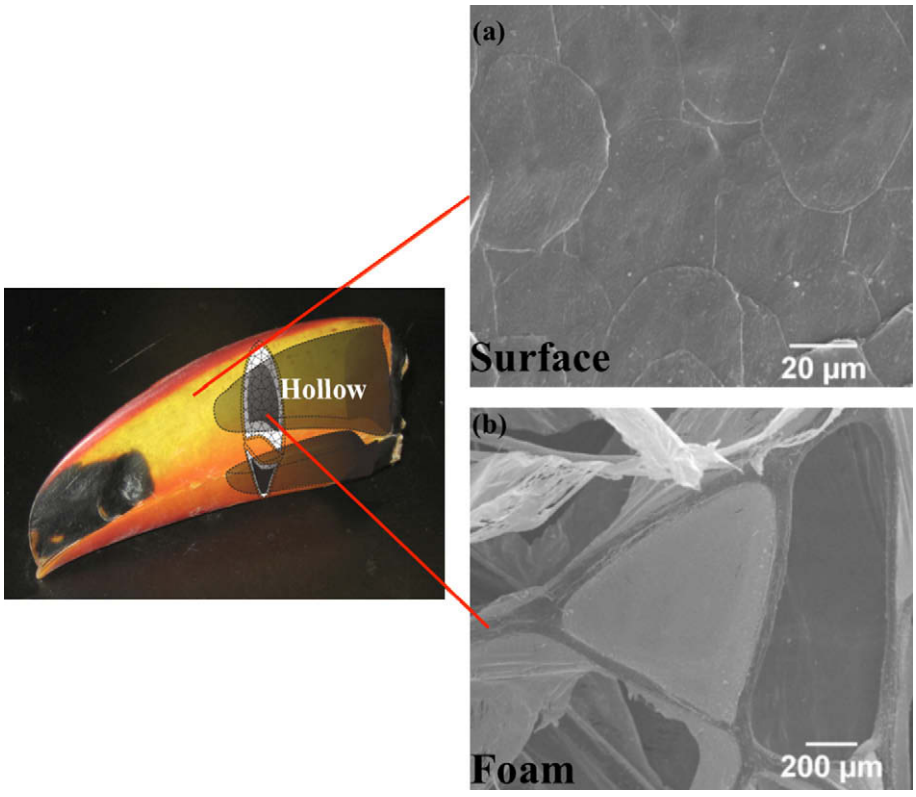

Fig. 2. Schematic overlay onto the photograph of the bill of the toco toucan superposing the interior structure onto exterior features with insets of scanning electron micrographs of (a) rhamphotheca on the exterior surface and (b) the trabecular, closed-cell form, as observed in the interior.

heca. In both specimens, the inter-tile spacing is conserved, measuring 18 ± 4 nm. Fig. 5(b) shows the longitudinally sectioned toucan rhamphotheca. The undulating cell boundary is observable as a dark curve in the micrograph. In the case of hornbill rhamphothec-

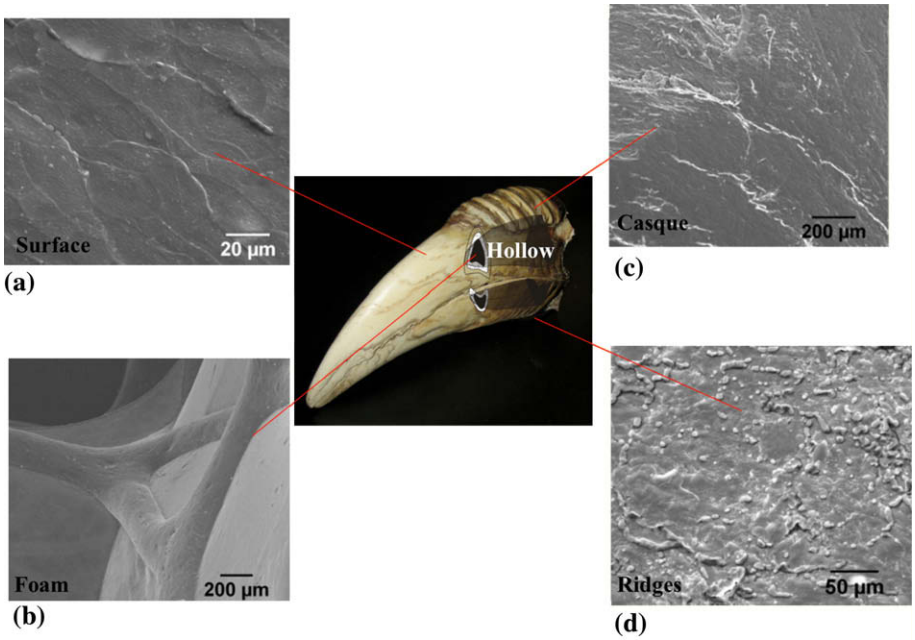

Fig. 3. Representation of the microstructure observed on and in the beak of the hornbill with scanning electron micrographs of (a) rhamphotheca, (b) interior foam and (c and d) rhinotheca at the casque. In (d), the distinguishable ridge-like surface structure of the casque is visible.

a, as demonstrated by Fig. 6(a), there are periodic voids along the cell boundaries.

The intermediate filaments are embedded in the keratin matrix and are sometimes branched. In both specimens, keratin filaments appear to be preferentially oriented within the cells and intercrossed or foam-like at the cell boundaries. The diameter of the β-keratin filaments in the toucan rhamphotheca is 7.5 ± 2.2 nm. The filaments run in parallel in the transversely sectioned beak keratin in Fig. 5(a). In the hornbill rhamphotheca, as shown in Fig. 6(b), the filaments are branched and create a foam-like network. The diameter of the hornbill keratin filaments is 10.7 ± 2.5 nm. In the longitudinal section, the hornbill keratin filaments are preferentially oriented within cells (Fig. 6(b)).

Dresp et al. [13,14] imaged intermediate filaments in penguin beak and reported a diameter of 3.5 nm. Fraser and Parry [15] reported the diameter of β-keratin filaments to be ∼4 nm. Our results are two to four times higher than these reported values [13–15]. This may be associated with the high degree of variability in diameter along the filament length and with tangling of filaments, or with variability between biological taxa.

3.1.3. Computed tomography

The toucan maxilla and mandible beaks reconstructed by the ray casting method are pictured in Fig. 7. The beak is colored with yellow by vtkColorTransferFunction. The length of the maxillary beak is 18.5 cm and that of the mandibular beak is 17 cm. The beak is longitudinally sectioned and the interior trabecular bone structure is visible in Fig. 7(b). For segmentation rendering of beak foams in Fig. 8, we used brown and white color for the distinction between bone and soft tissue, respectively. The foams are bisected at the center with proximal and distal views, which reveal a network of osteal rods comprising the foam interior. The toucan beak exterior is completely stripped and only the internal foam structure is reconstructed in Fig. 8(a). The volumetric rendering of hornbill rostrum depicts both keratinous rhamphotheca and foam interior. There is a secondary hollow region observed between the casque and the bony foam shown in Fig. 8(b). This secondary hollow region closes at the end of casque from proximal end. Because the lipid membranes were not detected by the X-ray computed tomography technique, it is possible that the casque may contain continuous membranes. However, considering that the casque of the hornbill has been associated with an acoustic function or syringeal signal amplification [16], we would not expect this to be the case. Some regions of the foam were rendered visible at the higher (27 μm) resolution of μ-CT. Edges of toucan foam and hornbill casque are shown in Fig. 9. The trabecular rods are connected to bony shell, which has a thickness of ∼150 μm in Fig. 9(a). The cell membranes are located at concave trabecular rods, indicated by arrows, although the membranes are not visible. The presence of membranes in toucan foam is difficult to detect even at 27 μm resolution. The casque region is shown at a resolution of 43 μm in Fig. 9(b). The bony exterior of the hornbill beak has a thickness of ∼300 μm. The thickness of the casques is ∼4 mm, and thickened keratin is connected to the bony exterior. The structure of hornbill trabeculae includes rod- and plate-like structures.

A comparative analysis of trabecular foam in both toucan and hornbill specimens was conducted by μ-CT measurements. Relevant parameters deduced from μ-CT measurements are reported in Table 1 (mean ± standard deviation), wherein the term "bone" applies to the mineralized collagen comprising the struts of the foam structure. The bone mineral density is approximately five times higher in hornbill foam than in toucan foam, and the bone volume fraction is an order of magnitude higher. The trabecular spacing for toucan foam is, on average, greater than for hornbill foam, but, as previously mentioned, the standard deviation for the distribution of toucan foam cell sizes is about 35%, compared to only about 10% for hornbill foam cells.

3.2. Mechanical properties of the beak

3.2.1. Micro- and nanoindentation

The microhardnesses of toucan and hornbill rhamphotheca, shown in Fig. 10(a), are comparable. However, there is a statistically highly significant difference in nanoindentation hardness, hornbill rhamphotheca hardness being twice that of toucan. Table 2 shows a summary of indentation results of keratinous rhamphot-

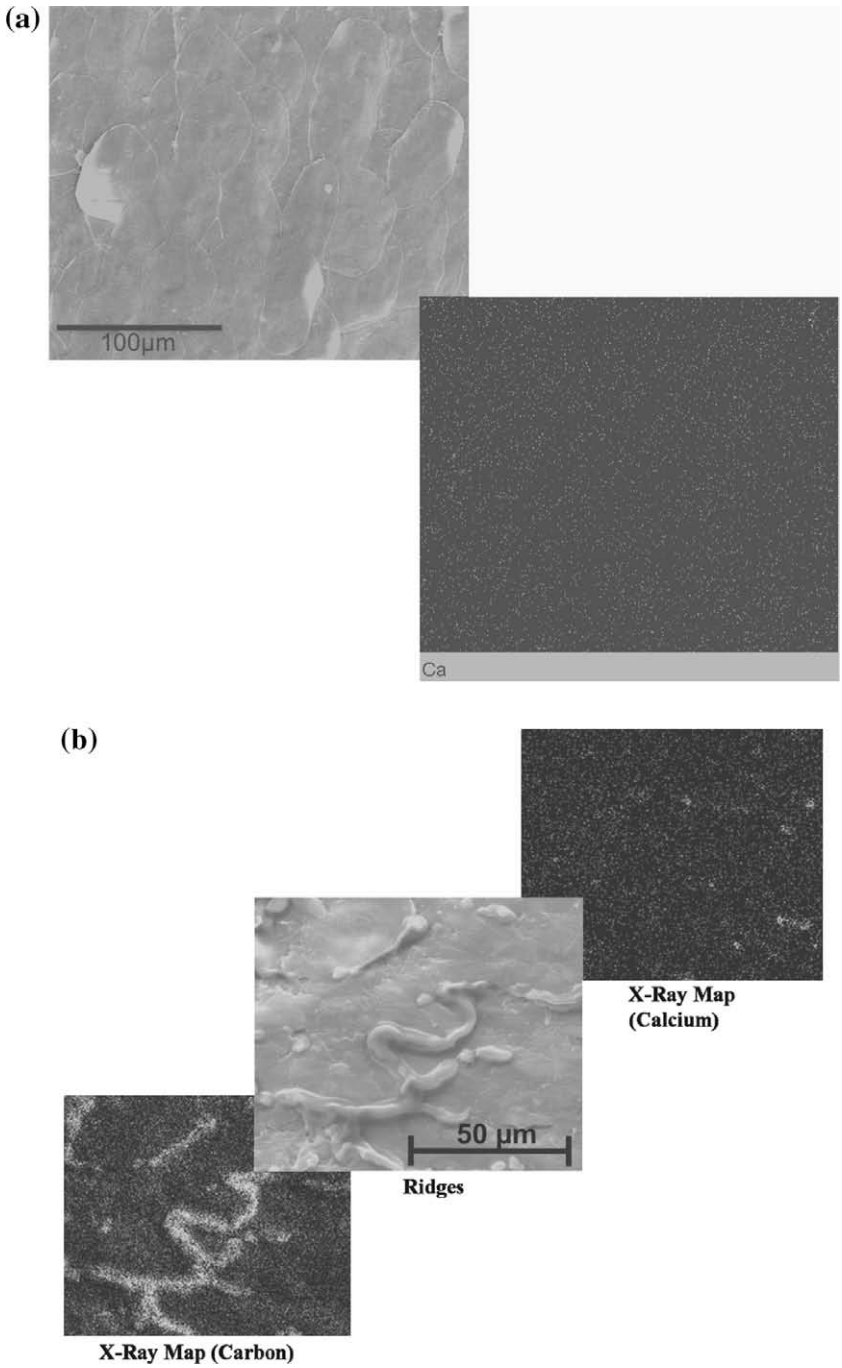

Fig. 4. Scanning electron micrographs accompanied by X-ray dot mapping depicting (a) the calcium distribution on toucan rhamphotheca and (b) the calcium distribution and carbon-rich ridges of the hornbill casque surface structure.

heca. The equivalent comparison for the trabeculae is illustrated in Fig. 10(b). Nanoindentation hardness values are almost twice as high as microhardness values. The hardness of hornbill trabeculae is 44% higher in macroindentation and 34% higher in nanoindentation than that of toucan trabeculae. We suggest that the higher hardness values for the hornbill trabeculae are a result of a greater degree of mineralization, as supported by μ-CT measurements. That the increased hardness of hornbill rhamphotheca, especially at nanoscale, is a result of a greater degree of mineralization is not supported by EDX data.

For keratin and bone samples of both taxa, the nanohardness values are significantly higher than the microhardness values. According to Rho et al. [17,18], in the case of bone, the higher nanoindentation values are caused by a scale dependence of the mineral–collagen interaction. The microhardness of the hornbill beak trabecula is comparable to that of avian humeral trabecular bone (~0.40 GPa) [19]. A summary of the hardness and reduced Young's modulus of beak trabeculae is listed in Table 3. We compared these with bone and antler, as they are other mineralized and collagenized biological materials for which hardness values have been reported in the literature. The microhardness of trabecular bone is reported to be ~0.3 GPa [20] and 0.34 GPa [21] in dry conditions. The nanoindentation results from Rho et al. [18] show that the hardness of trabecular bone in the transverse direction is

Table 1
μ-CT measurements of toucan and hornbill foam.

Attribute (dimensions)	Abbreviated nomenclature	Toucan foam	Hornbill foam
Bone mineral density (mg cc^{-1})	BMD	110 ± 5	497 ± 14
Bone volume fraction	BVF	0.024 ± 0.011	0.11 ± 0.03
Tissue mineral density (mg cc^{-1})	TMD	279 ± 22	900 ± 100
Bone surface:bone volume (mm^{-1})	BS/BV	8.3 ± 0.7	6.3 ± 1.6
Trabecular thickness (mm)	TbTh	0.24 ± 0.02	0.33 ± 0.07
No. of trabeculae per length (mm^{-1})	TbN	0.10 ± 0.05	0.33 ± 0.04
Trabecular separation (mm)	TbSp	6.4 ± 2.3	2.7 ± 0.3

0.56 GPa, with a Young's modulus of 16.6 GPa. The microhardnesses are 0.21 and 0.16 GPa for 3- and 5-year-old antler, respectively [22]. The microhardness of bone is close to that of hornbill trabeculae, while nanoindentation results for bone fall in the range of those values measured for both toucan and hornbill. The microhardness of antler is less than beak trabeculae, which might be associated with the mineral density.

3.2.2. Tensile response of rhamphotheca

Fig. 11(a) shows typical stress–strain curves of the beak keratin (rhamphotheca) of toucan and hornbill. Multiple trials (at least 5) were carried out for each orientation or condition. While the tensile strength and elongation of toucan rhamphotheca differ in the longitudinal and transverse directions, the Young's moduli are almost isotropic: 1.04 ± 0.06 GPa in the longitudinal direction and 1.12 ± 0.13 GPa in the transverse direction. In contrast, the tensile

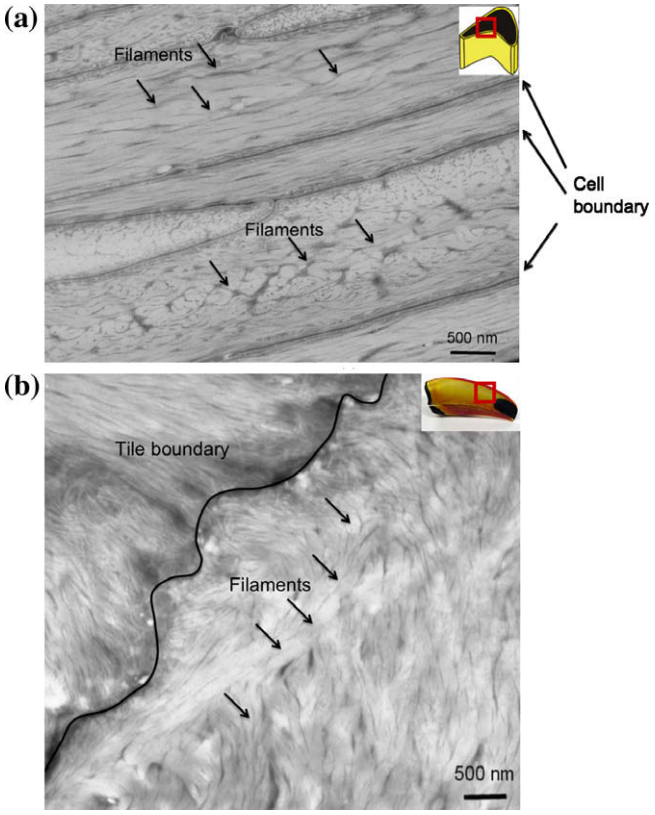

Fig. 5. Toucan rhamphotheca imaged by TEM in two orientations. (a) Cross-sectional view, as demonstrated by the schematic inset, reveals that the keratin tiles are lens-shaped, tapering in thickness at the edge. The filaments are indicated by arrows. (b) The lateral surface. Arrows indicate the filaments and tile boundaries are indicated by the black curve. The TEM images were acquired at 80 keV.

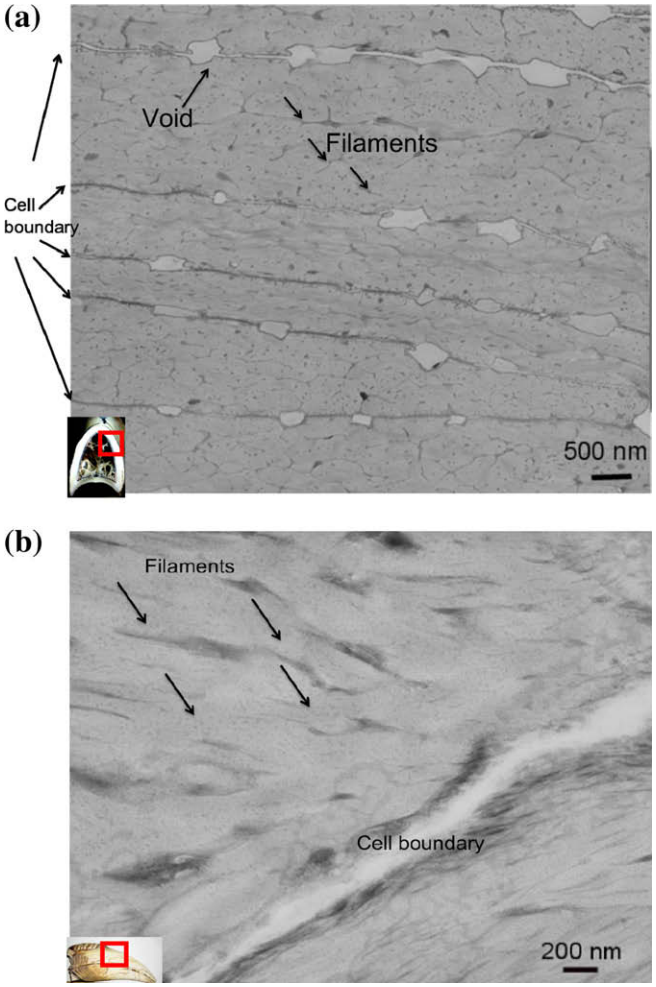

Fig. 6. TEM of hornbill rhamphotheca; (a) cross-section, the filaments are indicated by arrows and edge of keratin tiles become thin; (b) lateral surface, arrows indicates the filaments. Insets specify the surfaces that were imaged. The TEM images were acquired at 80 keV.

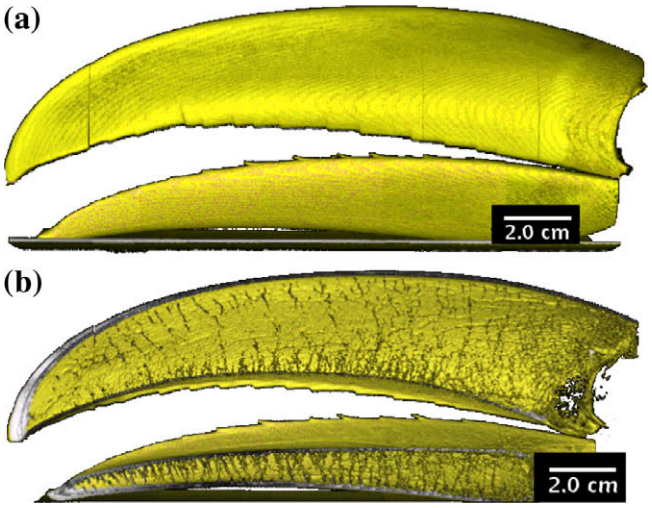

Fig. 7. Three-dimensional rendering of the maxillary and mandibular beaks of toucan generated by ray casting: (a) entire beak; (b) longitudinally sectioned beak. The dimensions of the images for the toucan maxilla are 121 × 156 pixels, with 1168 images, and for the toucan mandible 115 × 85 pixels, with 991 images.

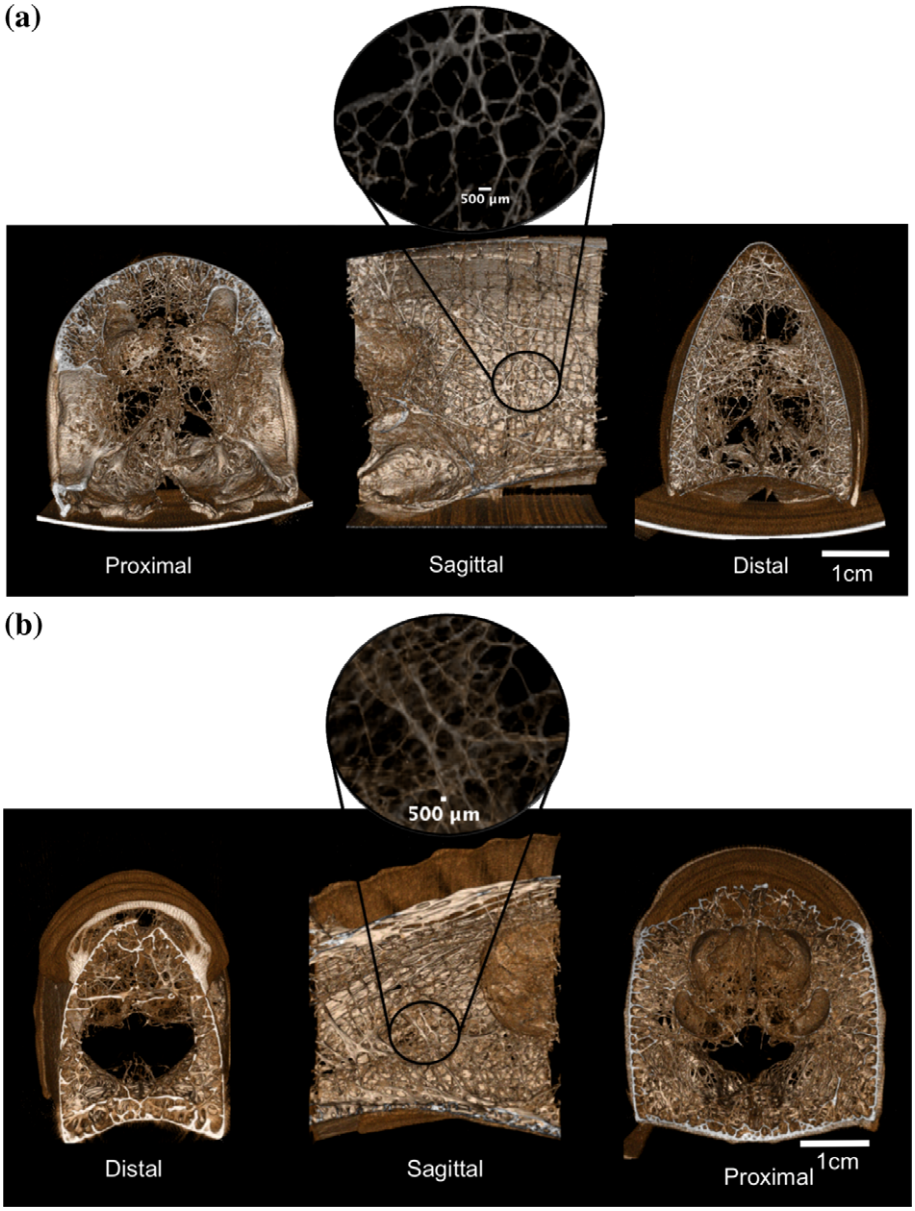

Fig. 8. Three-dimensional structure of foam generated by VTK at distal and proximal cross-sections as well as a sagittal view of the mid-region from 93 μm resolution μ-CT scans for: (a) toucan and (b) hornbill. A series of 435 images were used for the toucan and 430 images were used for the hornbill. The image size of the toucan is 225 × 255 pixels and that of the hornbill is 252 × 277 pixels.

response of hornbill rhamphotheca possibly exhibits anisotropic behavior in the longitudinal and transverse directions. The Young's moduli of hornbill rhamphotheca are 1.2 ± 0.3 GPa in the longitudinal direction and 0.81 ± 0.06 GPa in the transverse direction. The toucan rhamphotheca exhibits the highest tensile strength in the transverse direction, whereas for the hornbill the tensile strength in the longitudinal direction is twice the transverse. These differences in behavior of the rhamphotheca may be associated with the differences in keratin tile geometry in Fig. 12, as toucan scales were found to be typically regular and hexagonal, while hornbill scales were more irregular, being twice as long in one orientation than in the other.

3.2.3. Compressive response of beak foam

Fig. 11(b) shows typical compressive stress–strain curves of toucan and hornbill foam. The Young's modulus is determined from the slope at the onset of the curve. The long oscillatory region of the curve corresponds to collapse of individual cells by fracture of trabeculae. Foam densification (i.e. the abrupt raise in stress at the end of a plateau) initiates after the cells are completely collapsed and compacted. Despite differences in cell sizes and trabecular thickness, densification of foam, indicated by the rapid rise of the curve, for both toucan and hornbill beak starts at a strain of 0.9. This is due to comparable relative density of foam of both toucan and hornbill beaks.

The stress plateau of hornbill beak foam is six times higher than that of the toucan due to the higher modulus of hornbill trabeculae, since both foams have similar relative density. The nanoindentation results in Table 3 show that the modulus of hornbill trabeculae is almost twice that of toucan. This higher hardness is due to the greater degree of mineralization of the hornbill trabeculae, as corroborated by the bone mineral density data collected from μ-CT image analysis. The strength of the foams is dominated by the trabeculae, the contribution from the membranes being considered

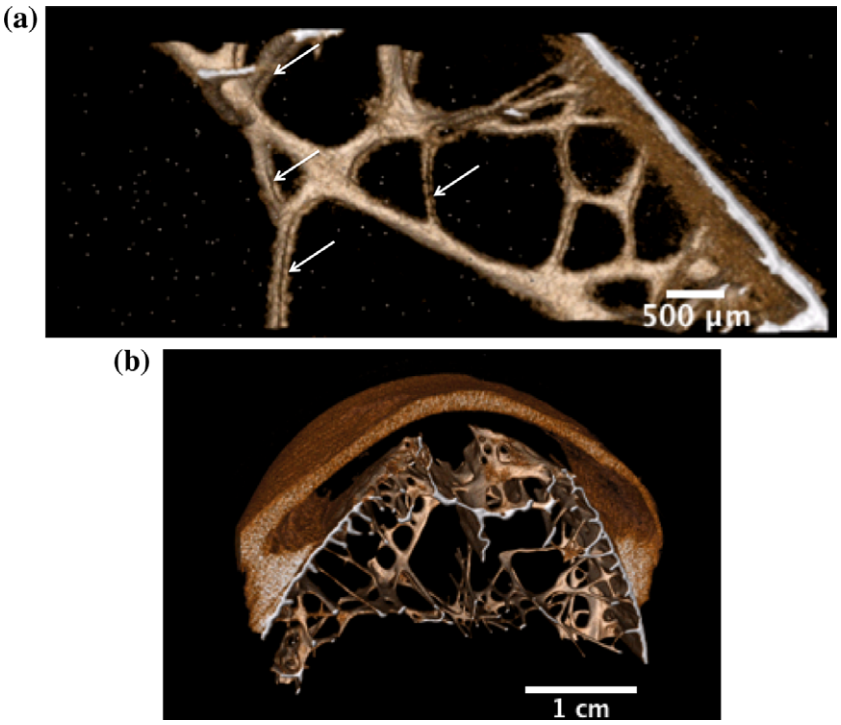

Fig. 9. Three-dimensional structure of beak foams generated by VTK: (a) toucan with 27 μm resolution μ-CT (arrows indicate concavity); (b) hornbill with 43 μm resolution μ-CT. A segment of toucan beak foam was scanned at a resolution of 27 μm. The image is 330 × 130 pixels, with 130 images. The hornbill casque was scanned at a resolution of 45 μm. The image is 312 × 237 pixels, with 80 images with 27 μm resolution μ-CT (arrows indicate concavity); (b) hornbill with 43 μm resolution μ-CT. A segment of toucan beak foam was scanned at a resolution of 27 μm. The image is 330 × 130 pixels, with 130 images. The hornbill casque was scanned at a resolution of 45 μm. The image is 312 × 237 pixels, with 80 images.

negligible especially due to the desiccated and pre-ruptured condition and the anticipated modulus mismatch between the membranes and the trabeculae.

3.3. Stability analysis

In our previous study, we used the Karam–Gibson model [23] to evaluate the sandwich design of the toucan beak [6]. The same model is applied here to compare hornbill and toucan beaks. We modeled the beaks as cylindrical beams at first. In order to apply the Karam–Gibson equations, we estimate the relative Young's modulus of the foam by the following Gibson–Ashby [12] equation for an open cell foam:

$$\frac{E^*}{E_{SF}} = C_1\left(\frac{\rho^*}{\rho_S}\right)^2 \tag{1}$$

where E^* is the Young's modulus of the foam, E_{SF} is the Young's modulus of the foam trabeculae, ρ^* is the density of the foam, ρ_s is the density of the foam material and C_1 is a material parameter ($\approx$1).

While the beak foam is structurally a closed-cell configuration, the mechanical response of beak foam behaves as an open cell foam in dry conditions, likely because many of the membranes sealing the cells are desiccated and ruptured by the time of testing.

The Karam–Gibson analysis [23] predicts the maximum compressive buckling load and bending moment of the sandwich-structured beam. In this model, both the foam and the solid shell are assumed to have the same Poisson's ratio: 0.3. Karam and Gibson [23] compared equivalent beams having the same weight and outer diameter, one in which the mass was concentrated entirely in the external shell and the other in which the mass was distributed between the external shell and the cellular core. Their calculations indicate the relative increase in load- and moment-bearing ability at the same weight. The expressions for load ratio, as modeled in Fig. 13(a), and relevant parameters thereof are described in Appendix A, Eqs. (i), (ii), and (iii). For bending, two limits are used by Karam and Gibson [23]: the Brazier moment (Eq. (iv) in Appendix A), which is the maximum value of flexure-resistive moment for a hollow cylinder, and the buckling moment (Eq. (v) in Appendix A), corresponding to the moment at which actual folding of the structure occurs.

Based on our results, we were able to estimate geometrical and material parameters for a simplified stability analysis of toucan and hornbill beaks as sandwich-structured composites. We obtained diameter-to-thickness ratios a/δ of 30–50 for toucan and of 15–30 for hornbill. We maintained the assumption of Karam and Gibson that, as a first approximation, $\upsilon_S = \upsilon^* = 0.3$. The ratio between the Young's moduli of the cellular material and the solid material was obtained for the open-cell geometry (Eq. (1)). The relative densities of the foam (ρ^*/ρ_s) were equal to 0.09 for toucan and 0.1 for hornbill.

Because the trabeculae of foam have a significantly higher reduced modulus than the keratin shell, we introduced a correction for this modulus mismatch. In order to establish the ratio of the foam's Young's modulus to that of the keratin shell, we used the Young's moduli listed in Table 4. The corrections for the relative Young's modulus are given by the following:

$$\frac{E^*}{E_S} = \frac{E^*}{E_{SF}} \times \frac{E_{SF}}{E_S} = 0.008 \times \frac{12.7}{6.7} = 0.015 \quad \text{(toucan)} \tag{2}$$

$$\frac{E^*}{E_S} = \frac{E^*}{E_{SF}} \times \frac{E_{SF}}{E_S} = 0.01 \times \frac{21.4}{9.3} = 0.023 \quad \text{(hornbill)} \tag{3}$$

where E_S is Young's modulus of shell and E_{SF} is as defined in Eq. (1).

The Karam–Gibson predictions of the loading and moment ratios as a function of a/δ for simplified toucan and hornbill beak pro-

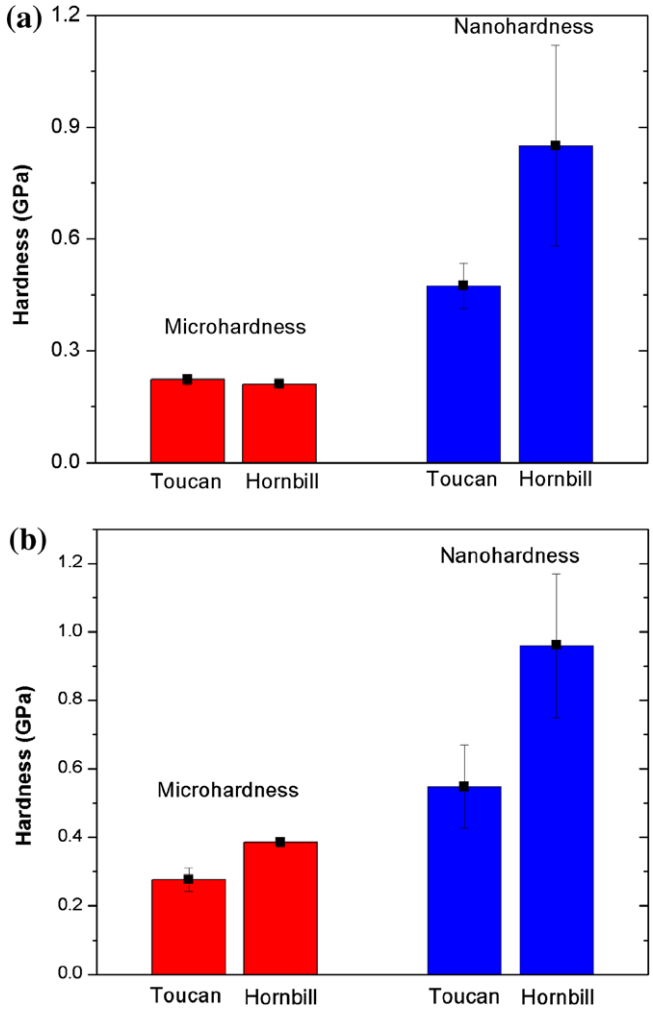

Fig. 10. Comparison between the hardness of toucan and hornbill beak components subject to loads by 100 gf at ambient conditions: (a) for non-melanized beak keratin, where the discrepancy between the nanohardness of the rhamphotheca between the toucan and hornbill is highly significant; and (b) for beak trabeculae, for which the the discrepancy in microhardness is highly significant, while that for nanohardness is not so. Error bars indicate standard deviation.

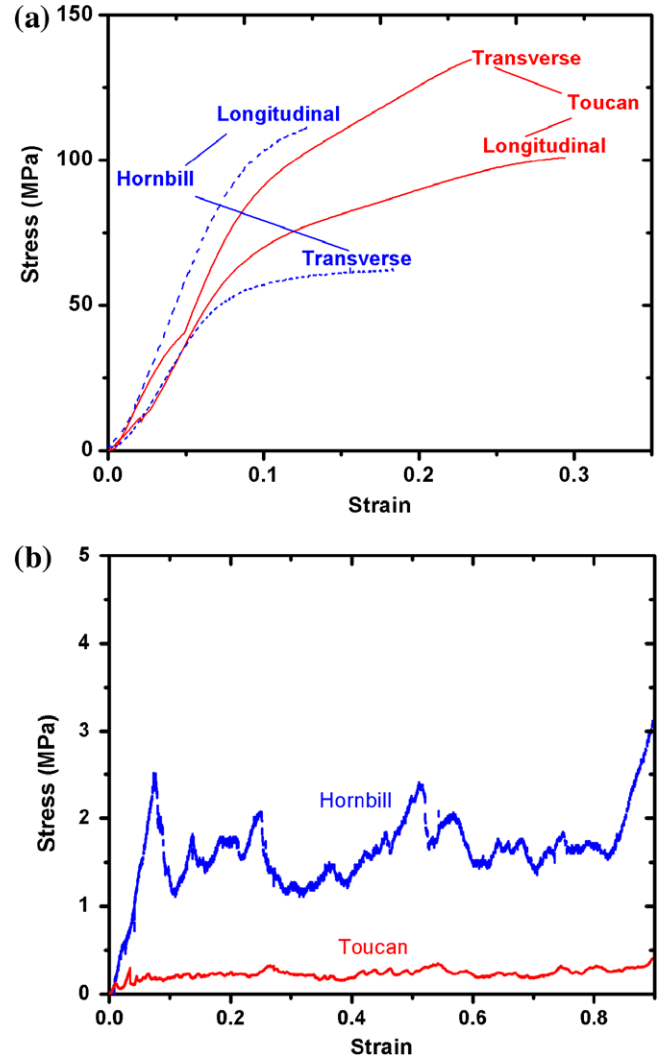

Fig. 11. Stress–strain curves: (a) rhamphotheca in tension; (b) sections of foam in compression. Densification is observed for both at 90% strain.

Table 2
Summary of micro- and nanoindentation results for rhamphotheca.

	Mean microhardness (GPa)	Mean nanohardness (GPa)	Reduced Young's modulus (GPa)
Toucan keratin	0.22 ± 0.012	0.50 ± 0.06	6.7 ± 0.8
Hornbill keratin	0.21 ± 0.015	0.85 ± 0.27	9.3 ± 1.8

Table 3
Summary of mean micro and nanohardness and reduced Young's modulus of foam trabeculae.

	Mean microhardness (GPa)	Mean nanohardness (GPa)	Reduced Young's modulus (GPa)
Toucan	0.27 ± 0.03	0.55 ± 0.12	12.7 ± 1.5
Hornbill	0.391 ± 0.014	0.94 ± 0.21	21 ± 5

totypes are plotted in Fig. 13. The range considered, from 10^0 to 10^2, represents the actual range of ratios for biological materials [23]. For the ratio of $a/\delta = 30–50$ as prescribed for toucan, the buckling load in compression actually decreases. The axial buckling load ratio, $P_0/(P_0)_{eq}$, for $E^*/E_s = 0.01–0.02$ is close to 0.5–0.6. However, the Brazier moment is significantly increased. The Brazier moment ratio is 3–5, while the buckling moment ratio is 0.9–1.5 for $a/\delta = 30–50$ and $E^*/E_s = 0.015$. Similarly, the ratio of $a/\delta = 15–30$ for hornbill, $P_0/(P_0)_{eq}$ for $E^*/E_s = 0.02–0.03$ is 0.7–0.8. The Brazier moment ratio is 3–6 and the buckling moment ratio is 1.5–1.7 for $a/\delta = 15–30$ and $E^*/E_s = 0.02–0.03$.

In the open cell configuration, the beak structure exhibits an improvement in Brazier moment. This indicates that the cellular sandwich structure increases the maximum flexural load of the beam. The improvement was not as significant as in the closed-cell configuration used in the previous analysis [6]. The Brazier moment is the most important structural parameter, defining the point beyond which the beak could not be loaded without incurring permanent damage.

3.4. Optimization analysis

In addition to the stability analysis, the Dawson–Gibson model [24,25] was applied to evaluate toucan and hornbill beak in uniaxial compressive loading and flexure. Dawson and Gibson [24,25]

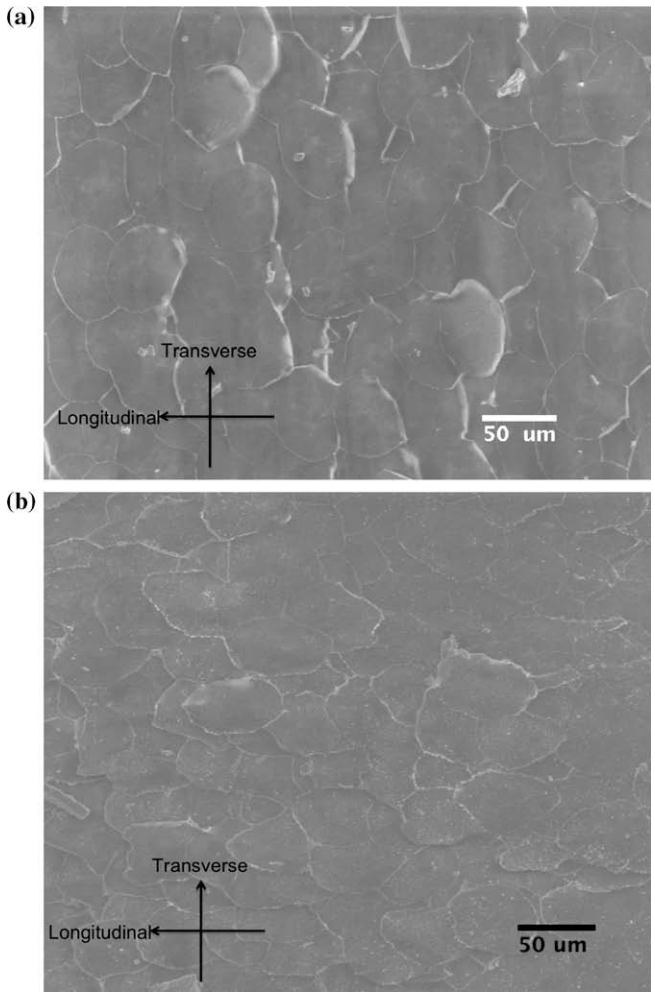

Fig. 12. Scanning electron micrograph of the rhamphotheca of (a) toucan and (b) hornbill depicting orientation with respect to the macrostructure of the beak.

incorporated the plasticity theory into the Karam–Gibson model and introduced two modes of failure: buckling failure and material failure. Equations of the model, governing buckling to material failure thresholds in axial loading conditions, are described in Appendix B. As for the stability analysis, because the shape of a bird's beak is homeomorphic with a hollow cylindrical beam, we modeled the beaks as such in our evaluation of toucan and hornbill optimization. The stability is described by the compressive loading and bending moment ratios of cylindrical shell to cylindrical shell with a hollow foam core, for which the shell and shell with foam core have approximately the same weight. The experimentally determined failure stress and Young's moduli of keratin and foam cores used in our calculations are listed in Table 4. The degree of ovalization ζ is 0.01 for both the toucan and hornbill beaks. The ratio of diameter of cylinder, a, to shell thickness, t, ranges from 15 to 50 for beaks.

Table 5 shows the modulus ratios according to experimental results and as predicted by the model. The lower modulus ratios in experimental results compared to analytical results might be associated with the sampling method for beak foam. The foam samples are fragile, and defects can be introduced when cutting and handling. Fig. 14 shows the uniaxial loading ratios with different materials as a function of modulus ratio. The transition point, from buckling failure to material failure, corresponds to the maximum optimal design of a sandwich-structured cylinder, in terms of the ratio of the modulus of the core to that of the cylindrical shell. After

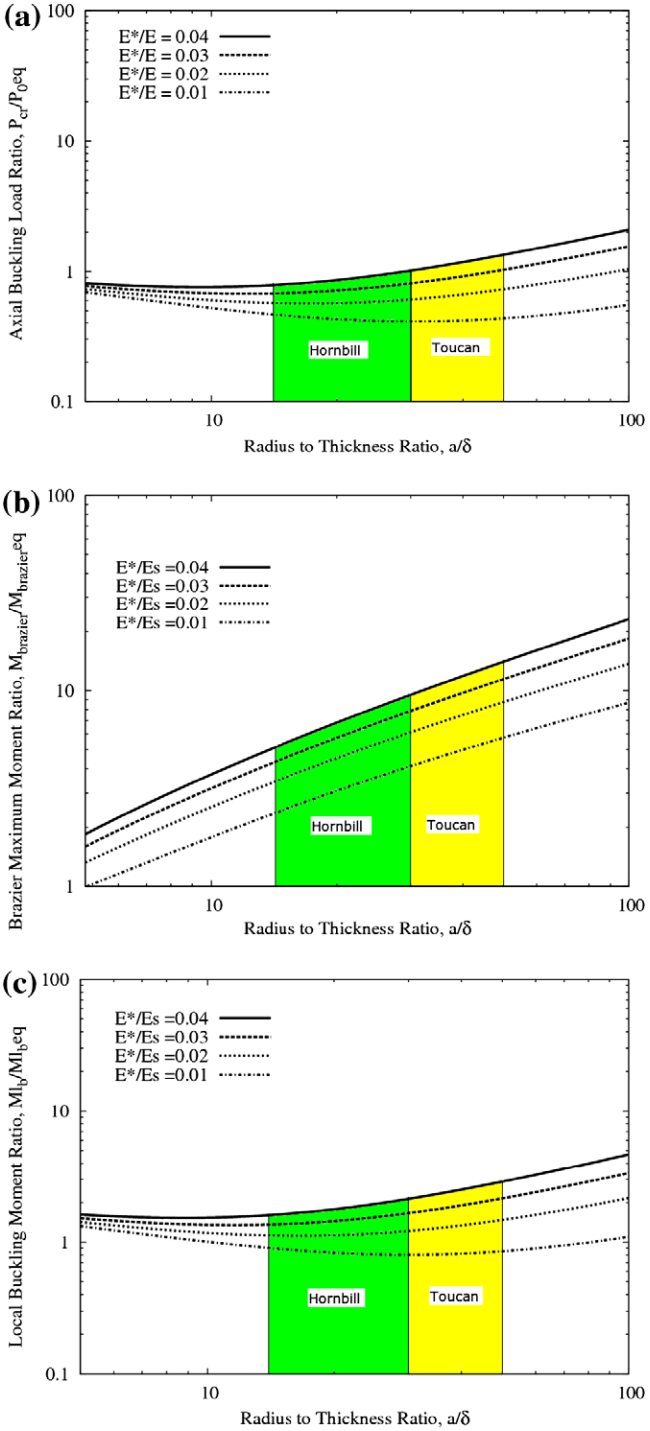

Fig. 13. Ratio of buckling load in uniaxial compression between a hollow circular shell with and without a cellular core at the same weight ($\rho^*/\rho = 0.1$). Ratio of (a) uniaxial compressive loading; (b) maximum (Brazier) moment; (c) local buckling moments.

Table 4
Material parameters used for optimization analysis of toucan and hornbill beaks.

	Shell modulus E_s (GPa)	Core modulus E^* (GPa)	Failure stress of shell σ_f (MPa)
Toucan beak	1.0	0.013	90
Hornbill beak	1.2	0.035	120

Table 5
Experimental and modeling results for optimum modulus ratios.

	Experimental results (E^*/E_s)	Compressive loading configuration $(E^*/E_s)_{P\text{-transition}}$	Bending configuration $(E^*/E_s)_{M\text{-transition}}$
Toucan beak	0.013	0.06	0.054
Hornbill beak	0.029	0.07	0.11

the transition point, the moment ratio of shell to that of shell with hollow core decreases as E^*/E_S ratio increases. The modulus ratios of the toucan and hornbill are considerably higher than for other synthetic sandwich composites. It should be noted that we considered $a/t = 100$ for this analysis and assumed that foam and shell are made from the same material, which we know not to be the case; however, the mechanical properties of the keratin shell and foam materials are within the same order of magnitude. Furthermore, while the ratio a/t of 100 is not typical for toucan and hornbill beaks, both achieve that ratio at the proximal terminus. This analysis shows that the toucan and hornbill beaks achieve higher resistance to uniaxial loading, especially at the base of the beak, compared to other synthetic materials.

4. Discussion

As expected, a number of similarities were observed in the structure and morphology of the beaks of the two taxa considered in this study. Both systems represent a sandwich-structured composite having a relatively thin, hard exterior encasing a relatively thick, low-density core consisting of bony trabeculae. On the surface, keratin tiles of both species are similar in dimension, and inter-tile spacing is conserved. While the beaks of the toucan and hornbill constitute the same proportion of the bird by mass, the hornbill beak has a higher apparent density.

On the rhamphotheca, we observed some differences in structure. While the keratin tiles on the surface of the toucan bill are regular polygons, those of the hornbill rhamphotheca are elongated in the longitudinal direction. Tensile testing results suggest mild anisotropy, favoring the longitudinal direction over the transverse. It has been reported that keratin deposition is directed from the proximal to the distal end and from the medial ridge toward the tomial edges [26]. The geometric anisotropy of the keratin tiles in the rhamphotheca of hornbill may indicate that the growth rate in the proximal to distal direction exceeds that in the transverse orientation of the beak. Whether this difference is related to a difference in feeding ecology or function of the beak is not known.

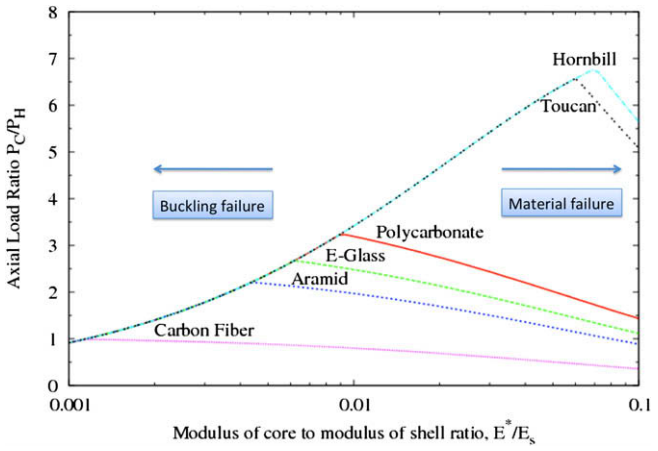

Fig. 14. Axial load ratio vs. modulus ratio, $a/t = 100$ (adapted from Fig. 3(b) of Dawson and Gibson [12]); transition from buckling to material failure occurs at a much higher normalized axial load for toucan and hornbill beaks than for synthetic sandwich structures.

Foam is at the core of both beaks. In compression testing, the onset of densification occurs at 90% for samples of foam collected from both taxa, and likewise relative density is conserved. The stress plateau is about six times higher for hornbill foam than for toucan foam. This could be related to the fivefold increase in bone mineral density measured by μ-CT image analysis for hornbill foam. Hornbill trabeculae are significantly harder than toucan trabeculae at the microscale. Furthermore, by μ-CT measurement, trabecular spacing in toucan foam varies by nearly 50% compared to the 10% standard deviation the spacing measured in hornbill foam. This translates into a large variability in cell size in toucan foam. If the cell edge length exceeds the mean length, then that edge may be subject to a larger bending moment and, therefore, higher stress. Based on a simplified stability analysis, hornbill beak is more resistive to uniaxial loading than toucan beak, while toucan beak is slightly more suitable for resisting flexural loads.

5. Conclusions

The results of this comparative study of toucan and hornbill beaks support the following conclusions:

- The structure of both the toucan and hornbill beak consists of a keratinous exterior and a bony foam interior. The rhamphotheca is composed of superposed keratin scales, with a diameter of approximately 50 μm in the case of toucan or 30 μm × 60 μm in the case of hornbill, and a thickness of 1 μm. TEM revealed branched intermediate filaments embedded in beak keratin matrix.
- The foam consists of the closed-cell system of rod-like trabeculae and thin membranes.
- The toucan rhamphotheca shows isotropic behavior while the hornbill rhamphotheca may be anisotropic in tension.
- The deformation behavior of the toucan and hornbill foams in compression is similar and exhibits features of both brittle and ductile bending.
- The Karam–Gibson analysis proves that the cellular core in toucan and hornbill beaks serves to increase the resistance to bending. This is an increase to bending resistance compared to that conferred by a hollow cylinder of the same mass, devoid of the foam core, subject to the same uniaxial compressive load.
- The beak is mostly loaded in bending in foraging and fencing activities, and therefore, the three to sixfold increase in Brazier bending moment more than compensates the loss of compressive strength (~50%).
- The optimal point analysis in uniaxial compressive loading and bending moment of toucan and hornbill beaks was carried out using the Dawson–Gibson approach. The hornbill beak has a higher modulus ratio than toucan beak, according to this analysis.

Acknowledgements

We acknowledge those who furnished the bird beaks: Jerry Jennings of the Emerald Forest Birds Gardens and, especially, Michael Mace of the San Diego Wild Animal Park, who supplied, free of charge, hornbill beaks for this study. This research was supported by the National Science Foundation, Division of Materials Research, Biomaterials Program (Grant DMR 0510138). We thank Evelyn York at the Scripps Institute of Oceanography (analytical facilities)

for assisting with SEM and Professor Robert Mattrey and staff scientist Jacqueline Corbeil at the Moores Cancer Center at UCSD for CT scanning equipment access and consulting. Mason Mackey helped us to conduct TEM analysis at the National Center for Microscopy and Image Research Facility (NCMIR) at UCSD. Our special gratitude goes to Professor Franck Talke and his student Y.C. Yoon for allowing and supervising equipment access for the nanoindentation tests. We thank Dr. Bimal Kad for allowing us to carry out the mechanical tests, using the Universal Testing Machine, in his laboratory. We also thank two anonymous reviewers, who contributed to the improvement in the quality of our paper.

Appendix A. Karam–Gibson stability analysis

For axial loading, the ratio between the compressive force for the cellular P_{cr} and hollow cylinders $(P_0)_{eq}$ is:

$$\frac{P_{cr}}{(P_0)_{eq}} = \frac{\left[1 + 5\frac{\lambda_{cr}}{\delta}\frac{E^*}{E_S}\frac{\rho^*}{\rho_S}\left(1 - 2.5\frac{\lambda_{cr}/\delta}{a/\delta}\right)\right]f}{0.605\left[1 + 5\frac{\lambda_{cr}}{\delta}\frac{\rho^*}{\rho_S}\left(1 - 2.5\frac{\lambda_{cr}/\delta}{a/\delta}\right)\right]^2} \quad \text{(i)}$$

where a is the cylinder diameter and δ is the cylinder thickness. The parameter λ_{cr} represents a critical instability wavelength, which is equal to (Eq. (7) from Karam and Gibson [23]):

$$\lambda_{cr} = \frac{\delta}{\left[12(1-\upsilon_S^2)\right]^{1/4}}\left(\frac{a}{\delta}\right)^{1/2} \quad \text{(ii)}$$

The parameter f is equal to (Eq. (9) from Karam and Gibson [23]):

$$f = \frac{1}{12(1-\upsilon^2)}\frac{a/\delta}{(\lambda_{cr}/\delta)^2} + \frac{(\lambda_{cr}/\delta)^2}{a/\delta} + \frac{2E^*/E_S}{(3-\upsilon^*)(1+\upsilon^*)}\left(\frac{\lambda_{cr}}{\delta}\right)\left(\frac{a}{\delta}\right) \quad \text{(iii)}$$

The ratio of the Brazier moments between the cellular M_{Br} and hollow beams $(M_{Br})_{eq}$ is:

$$\frac{M_{Br}}{(M_{Br})_{eq}} = \frac{\left[1 + 1.747\left(\frac{a}{\delta}\right)^3\frac{E^*}{E_S}\frac{5\lambda_{cr}/\delta}{a/\delta}\left(2 - \frac{5\lambda_{cr}/\delta}{a/\delta}\right)\right]^{1/2}}{\left[1 + \frac{5\lambda_{cr}}{\delta}\frac{\rho^*}{\rho_S}\left(1 - \frac{5\lambda_{cr}/\delta}{2a/\delta}\right)\right]^2} \times \frac{\left\{1 + \frac{5}{4}\frac{\lambda_{cr}}{\delta}\frac{E^*}{E_S} + 0.095\frac{a}{\delta}\frac{E^*}{E_S}\left[1 - \left(1 - \frac{5\lambda_{cr}/\delta}{a/\delta}\right)^4\right]\right\}^{3/2}}{\left(1 + \frac{5}{4}\frac{E^*}{E_S}\frac{\lambda_{cr}}{\delta}\right)} \quad \text{(iv)}$$

The ratio of the buckling moments, $M_{lb}/(M_{lb})_{eq}$, is given by (Eq. (35) from Karam and Gibson [23]):

$$\frac{M_{lb}}{(M_{lb})_{eq}} = \frac{\left(1 + 1.25\frac{E^*}{E_S}\frac{\lambda_{cr}}{\delta}\right)\left(1 + \frac{0.12\frac{E^*}{E_S}\frac{\lambda_{cr}}{\delta}}{1+1.25\frac{E^*}{E_S}\frac{\lambda_{cr}}{\delta}} - \frac{3}{2}\zeta\right)(1-3\zeta)f}{0.312\left[1 + 5\frac{\lambda_{cr}}{\delta}\frac{\rho^*}{\rho_S}\left(1 - 2.5\frac{\lambda_{cr}/\delta}{a/\delta}\right)\right]^2(1-\zeta)} \quad \text{(v)}$$

The parameter ζ represents a correction for the decrease in the moment of inertia produced by the ovalization of the anular cross-section. We used $\zeta = 0.01$ in this analysis.

Appendix B. Dawson–Gibson optimization analysis

The transition from buckling failure to material failure in uniaxial compression is given by:

$$\left(\frac{E^*}{E_S}\right)_{\text{P-transition}} = \left(\frac{2}{3}\right)(1+\nu_c)(3-\nu_c)\left(\sqrt{1-\nu^2}\right)\left(\frac{\sigma_f}{E_S}\right)^{3/2} \quad \text{(vi)}$$

where E^* is the core modulus, E_S is the shell modulus, ν and ν_c are Poisson's ratios of the shell and the core, respectively, and σ_f is the failure stress of the shell.

The buckling failure in uniaxial loading is described by:

$$\left(\frac{P_C}{P_H}\right)_{\text{transition}} = \frac{\sigma_f a t\sqrt{3(1-\nu^2)}}{E_S t_{eq}^2} \quad \text{(vii)}$$

$$\text{for} \quad \left(\frac{E^*}{E_S}\right) > \left(\frac{2}{3}\right)(1+\nu_c)(3-\nu_c)\left(\sqrt{1-\nu^2}\right)\left(\frac{\sigma_f}{E_S}\right)^{3/2}$$

where the equivalent thickness of the hollow cylinder t_{eq} and the thickness of the compliant cellular core t_c are:

$$t_{eq} = t\left(1 + \frac{t_c}{2t}\frac{\rho^*}{\rho_S}\left[2 - \frac{t_c}{a}\right]\right) \quad \text{(viii)}$$

$$t_c = 5\left[\frac{(3-\nu_c)(1+\nu_c)}{12(1-\nu^2)}\right]^{\frac{1}{3}}\left[\frac{E_S}{E^*}\right]^{\frac{1}{3}}t \quad \text{(ix)}$$

where $\upsilon_S = \upsilon^* = 0.3$.

The material failure in uniaxial loading is:

$$\left(\frac{P_C}{P_H}\right)_{\text{transition}} = \frac{2.27 a t(1-\nu^2)^{1/6}}{\left[(3-\nu_c)(1+\nu_c)\frac{E_S}{E^*}\right]^{2/3}t_{eq}^2} \quad \text{(x)}$$

$$\text{for} \quad \left(\frac{E^*}{E_S}\right) < \left(\frac{2}{3}\right)(1+\nu_c)(3-\nu_c)\left(\sqrt{1-\nu^2}\right)\left(\frac{\sigma_f}{E}\right)^{3/2} \quad \text{(xi)}$$

The transition in bending configuration is described by:

$$\left(\frac{E^*}{E_S}\right)_{\text{M-transition}} = \left(\frac{2}{3}\right)(1+\nu_c)(3-\nu_c)\left(\sqrt{1-\nu^2}\right)\left(\frac{\sigma_f}{(1-\frac{3}{2}\zeta)E_S}\right)^{3/2} \quad \text{(xii)}$$

where ζ is the ovalization of beam at local buckling.

Appendix C. Figures with essential colour discrimination

Certain figures in this article, particularly Figures 1, 2, 3, 5, 6, 7, 8, 9, 10, 11, 13 and 14, are difficult to interpret in black and white. The full colour images can be found in the on-line version, at doi:10.1016/j.actbio.2009.08.026.

References

[1] Meyers MA, Lin AY, Seki Y, Chen PY, Kad B, Bodde S. Structural biological composites: an overview. JOM 2006;58:35–41.
[2] Meyers MA, Chen PY, Lin AYM, Seki Y. Biological materials: structure and mechanical properties. Prog Mat Sci 2008;53:1–206.
[3] Vincent JFV. Structural biomaterials. Princeton, NJ: Princeton University Press; 1990.
[4] Chen PY, Lin AYM, Lin YS, Seki Y, Stokes AG, Meyers MA, et al. Structure, function and mechanical properties of selected biological materials. J Mech Behav Biomed Mat 2008;1:208–26.
[5] Chen PY, Lin AYM, Stokes AG, Seki Y, Bodde SG, McKittrick J, et al. Structural biological materials: overview of current research. JOM 2008;60:23–32.
[6] Seki Y, Schneider MS, Meyers MA. Structure and mechanical behavior of a toucan beak. Acta Mat 2005;3:5281–96.
[7] Seki Y, Kad B, Benson D, Meyers MA. Toco toucan beak; structure and mechanical properties. Mat Sci Eng C 2006;26:1412–20.
[8] Hillerton JE, Reynolds SE, Vincent JFV. On the indentation hardness of insect cuticle. J Exp Biol 1982;96:45–92.
[9] Bonser RCH, Witter MS. Indentation hardness of the bill keratin of the European starling. Condor 1996;95:736–8.
[10] Hulscher JB. Growth and abrasion of the oystercatcher bill in relation to dietary switches. Neth J Zool 1985;35:124–54.
[11] The VTK User's guide, 5th ed. Kitware, Inc; 2006.
[12] Gibson LJ, Ashby MF. Cellular solids: structure and properties. 2nd ed. Cambridge: Cambridge University Press; 1997.
[13] Dresp B, Jouventin P, Langley K. Ultraviolet reflecting photonic microstructures in the king penguin beak. Biol Lett 2005;22:310–3.
[14] Dresp B, Langley K. Fine structural dependence of ultraviolet reflections in the king penguin beak horn. Anat Rec A 2006;288A:213–22.
[15] Fraser RDB, Parry DAD. The molecular structure of reptilian keratin. Int J Biol Macro 1996;19:207–11.
[16] Kemp A, Woodcock M. The hornbills: bucerotiformes. New York: Oxford University Press; 1995.

[17] Rho JY, Tsui TY, Pharr GM. Elastic properties of human cortical and trabecular lamellar bone measured by nanoindentation. Biomaterials 1997;18:1325–30.
[18] Rho JY, Roy ME, Tsui TY, Pharr GM. Elastic properties of microstructural components of human bone tissue as measured by nanoindentation. J Biomed Mat Res 1999;45:48–54.
[19] Bonser RHC. Longitudinal variation in mechanical competence of bone along the avian humerus. J Exp Biol 1995;198:209–12.
[20] Todoh M, Ihara M, Matsumoto T, Tanaka M. Relationship between mechanical property of cancellous bone and hardness of trabeculae. JSEM Int J C 2004;40:1075–8.
[21] Dall'Ara E, O¨hman C, Baleani M, Viceconti M. The effect of tissue condition and applied load on Vickers hardness of human trabecular bone. J Biomech 2007;40:3267–70.
[22] Evans GP, Behiri JC, Currey JD, Bonfield W. Microhardness and Young's modulus in cortical bone exhibiting a wide range of mineral volume fractions, and in a bone analogue. J Mat Sci 1990;1:38–43.
[23] Karam GN, Gibson LJ. Elastic buckling of cylindrical shells with elastic cores-I. Anal Int J Sol Struct 1995;32:1259–83.
[24] Dawson MA, Gibson LJ. Biomimetics: extending nature's design of thin wall shells with circular cores. In: Brebbia CA, editor. Design and nature III: comparing design in nature with scientific and engineering. Boston: WIT Press; 2006. p. 145–55.
[25] Dawson MA, Gibson LJ. Optimization of cylindrical shells with compliant cores. Int J Solid Struct 2007;44:1145–60.
[26] Altman RB, Clubb SL, Dorrestein GM, Quesenberry K. Avian medicine and surgery. Pennsylvania, PA: WB Saunders & Co.; 1997.